Water Resources Research

RESEARCH ARTICLE
10.1029/2019WR024777

Spatiotemporal Dynamics of the Active Perirheic Zone in a Natural Wetland Floodplain

T. Berezowski[1,2], D. Partington[2], J. Chormański[3], and O. Batelaan[2]

[1]Faculty of Electronics, Telecommunication and Informatics, Gdansk University of Technology, Gdansk, Poland, [2]National Centre for Groundwater Research and Training, College of Science and Engineering, Flinders University, Adelaide, South Australia, Australia, [3]Institute of Environmental Engineering, Warsaw University of Life Sciences – WULS, Warsaw, Poland

Key Points:
- An integrated hydrological model with a Hydraulic Mixing-Cell method identifies the active perirheic zone
- Active perirheic zone is highly dynamic; geochemical processes occur over a larger area than considered under a static concept
- The active perirheic zone depends on hydrological and climatological conditions, making it vulnerable to climate change

Supporting Information:
- Supporting Information S1

Correspondence to:
T. Berezowski,
tomberez@eti.pg.edu.pl

Citation:
Berezowski, T., Partington, D., Chormański, J., & Batelaan, O. (2019). Spatiotemporal dynamics of the active perirheic zone in a natural wetland floodplain. *Water Resources Research*, *55*, 9544–9562. https://doi.org/10.1029/2019WR024777

Received 17 JAN 2019
Accepted 24 OCT 2019
Accepted article online 9 NOV 2019
Published online 20 NOV 2019
Corrected 17 FEB 2020

This article was corrected on 17 FEB 2020. See the end of the full text for details.

Abstract The ecologically and biogeochemically significant perirheic zone is a part of the floodplain where waters originating from both the river and adjacent floodplain are present. In this study, we investigate the spatiotemporal dynamics of the active perirheic zone, that is, river and floodplain waters and their transient mixing extent. This is achieved by using the Hydraulic Mixing-Cell method, a complement to a fully integrated surface-subsurface hydrological model, in the Biebrza catchment, northeast Poland. The model performance is verified against hydrological and hydrochemical data sets. The simulations show that overbank flooding river water is unable to penetrate deeply into the floodplain due to the presence of floodplain water. However, the active perirheic zone moves toward the floodplain and back within a buffer of at least 1 km from its initial position located approximately 0 to 2.5 km from the Biebrza River. The active perirheic zone is also present further away from the river due to the discharge of tributaries and surface runoff. The active perirheic zone exhibits multidirectional movement and can reappear in different places after a period of time. Effectively, during the flooding period, the active perirheic zone moves over 38% of the floodplain area, while the maximum daily extent is 24% of the floodplain. These dynamics imply that biogeochemical processes related to the perirheic zone, for example, denitrification, also vary in space and time. Due to the strong correlation of the perirheic zone extent with the meteorologically dependent variables, especially the snowmelt water extent, it is vulnerable to climate change.

1. Introduction

The perirheic zone, complementary to the hyporheic zone, is a part of the floodplain where river and floodplain waters from various sources are present (Mertes, 1997). The floodplain water sources are rainfall, snowmelt, groundwater, and river water from tributaries (Fritz et al., 2018), which differ in chemical composition, sediment load and momentum compared to the water in the main river. During the buildup of a flood, the floodplain water is connected to the river water and forms a distinguishable transient mixing frontier, that is, the active perirheic zone. The presence of an active perirheic zone implies that waters from sources of entirely different makeup appear next to or after one another and constitute environmental gradients.

Originally, Mertes (1997) showed that for the world's major floodplains the significance of the perirheic zone was that it prevented river water from reaching remote areas of the floodplain. This observation was contrary to the flood pulse concept (Junk et al., 1986), which puts the river water as a major donor of sediments to the floodplain. In a number of recent studies hydrological, ecological, geomorphological and biogeochemical processes were shown to be related to the perirheic zone. Chormański et al. (2011) identified zones of water from different sources in the Biebrza River floodplain (Poland) and related them to the vegetation patterns. Keizer et al. (2014), in a follow-up study, further investigated the zones and questioned the relevance of the flood pulse concept for temperate zone floodplains. Park and Latrubesse (2015) suggested that the mixing of black and white waters from the Solimões-Amazon and Negro Rivers constitutes various habitats and influences the hydrogeomorphological patterns. Shellberg et al. (2013) showed that water from different floodplain sources can control different erosion processes in the Mitchell River floodplain. Aalto et al. (2003) indicated that coexistence of sediment-free floodplain water next to the sediment-rich river water can inhibit crevasse splays during Amazon floods. Jones et al. (2014) pointed out the importance of taking into account the perirheic zone for analyzing biogeochemical processes in the Atchafalaya River floodplain

(USA). They concluded that more biogeochemical processing, including denitrification, occurred within the flow-through wetland than in the backwater zones. Further, studies showed that denitrification was stimulated by the oxic-hypoxic gradient occurring at the boundary between the river and floodplain waters and also when river water covered the floodplain water in the floodplains with high connectivity (Forshay & Stanley, 2005; Jones et al., 2014; Racchetti et al., 2011; Scaroni et al., 2011). Finally, a study by Scott et al. (2014) conducted in the Atchafalaya floodplain confirmed the importance of the flow-through zone and suggested that floodplain management leading to diversion of this zone over the backwater wetlands could decrease the nitrate loads to the Gulf of Mexico. These studies clearly show the significance of the active perirheic zone. However, thus far, no study has investigated the continuous spatiotemporal dynamics of the active perirheic zone, which is important for quantifying the time-variant area in which perirheic-related processes occur. Moreover, there is a clear lack of a proper tool allowing modeling and identification of how the zone develops, persists and recedes and the role of various water sources in these dynamics.

So far, delineating the extent of a particular water source is achieved either by field sampling or remote sensing (Mertes, 2000). The aforementioned studies used both approaches as they are useful in identifying the state for one or more time snapshots acquired during a field campaign, or a satellite overpass. However, these approaches do not provide the full dynamics in space and time for the river water, floodplain water and active perirheic zone. The limitation in obtaining the full dynamics is due to the field sampling approach providing spatially discrete results and the remote sensing approach being reliable only with deep, open water areas under no cloud coverage. Both approaches can provide near-continuous data in time. However, obtaining a high temporal resolution for field sampling implies high labor costs, whereas remote sensing compromises higher temporal resolution with lower spatial resolution. Nonetheless, spatially and temporally continuous data would be highly beneficial for better understanding processes related to the occurrence of the perirheic zone, or for simulating change scenarios, which are critical for improving floodplain management.

Hydrodynamic models have been used to attempt to map river water extents on floodplains. For example, Keizer et al. (2014) related the water chemistry patterns with flood exceedance probability maps determined by hydraulic modeling. Their results showed good spatial correspondence between the sampling points classified as river water and the frequently flooded areas; however, only during high river discharge conditions. The use of floodplain-oriented hydrodynamic models provides insight into both river and floodplain water extents. For example the LISFLOOD-FP model (Bates & De Roo, 2000), which calculates river-floodplain fluxes and accounts for other fluxes (e.g., precipitation, evapotranspiration, groundwater, or tributaries). A recent example is a study by Rudorff et al. (2014a) who quantified river-floodplain water fluxes and inundation extent for the Amazon River. Their modeling approach was, however, not able to provide the extent of the river and floodplain water separately. Rudorff et al. (2014b) indicate an important limitation of their modeling approach: The groundwater fluxes are estimated with empirical formulas and accounting for infiltration would require "sophisticated" groundwater modeling. Notably, Wilson et al. (2007) identified similar limitations in an earlier study conducted in the Amazonian floodplain, where the simulated inundation area was over-predicted due to a lack of included floodplain hydrological processes (infiltration and evaporation) and detailed drainage network in the model formulation.

To overcome the limitations of 2-D hydrodynamic models, when surface-subsurface fluxes and feedbacks are important, an integrated surface-subsurface hydrological model (ISSHM) (Sebben et al., 2013), for example, InHM (VanderKwaak & Loague, 2001), ParFlow (Kollet & Maxwell, 2006), and HydroGeoSphere (Brunner & Simmons, 2012; Hwang et al., 2014) can be used to model floodplain hydrology. Inspired by the Freeze and Harlan (1969) blueprint, ISSHMs simulate both 2-D surface water flow and 3-D variably saturated subsurface flow. An advantage of such a formulation is that the floodplain surface water - groundwater flux is computed implicitly based on hydraulic head gradients so that explicit surface-subsurface boundary conditions do not have to be prescribed.

Accounting for the full array of hydrological fluxes can be accomplished with the aforementioned ISSHM model codes, analyzing these fluxes in details is more complex and received relatively little attention. The Hydraulic Mixing-Cell (HMC) method (Partington et al., 2011) is a straightforward approach to analyze these fluxes, which applies to any hydrological model that computes local fluid mass balances. This method was originally developed to identify streamflow generation mechanisms and their contribution to the streamflow hydrograph (Partington et al., 2013), for use in assessment of baseflow contributions to streamflow (Li et al., 2013, 2014, 2015; Partington et al., 2012), for exploration of tracer interpretation

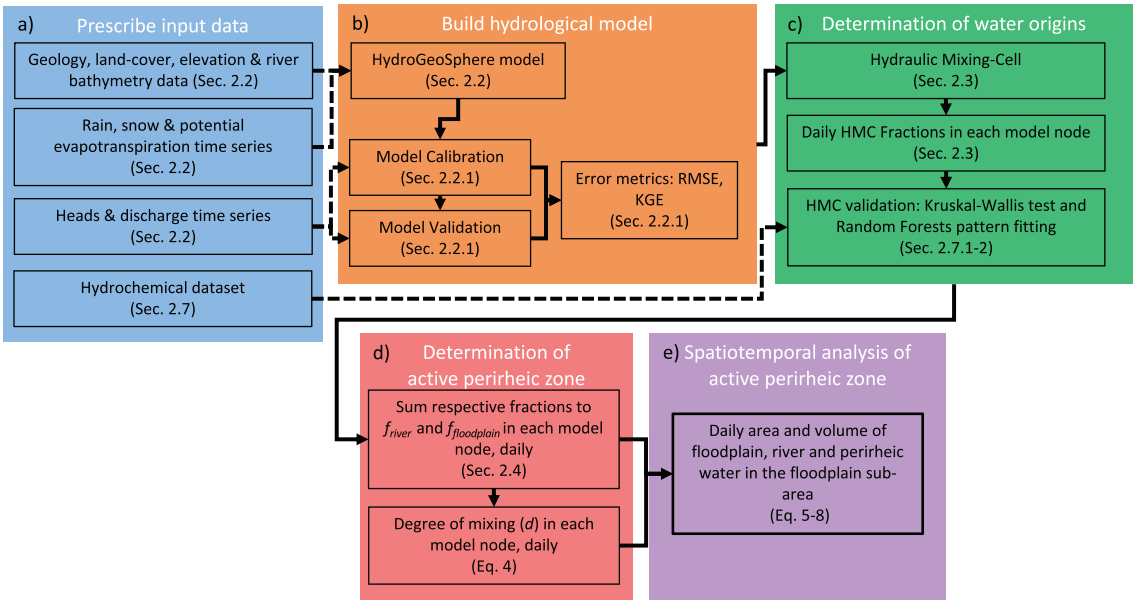

Figure 1. Flowchart of methods used in this paper to investigate the spatiotemporal dynamics of the active perirheic zone.

(Liggett et al., 2013, 2015), and in assessing contributions of various water sources to groundwater extractions (Schilling et al., 2017). The method traces the evolution of water from predefined sources, for example, river water discharge versus direct precipitation, in each cell of a model. Hence, it can be used to identify flood inundation generation mechanisms including spatiotemporal dynamics of the active perirheic zone.

Using a combination of numerical modeling, hydrological flux tracking and statistical analysis, this study aims to quantify the spatiotemporal dynamics of the active perirheic zone in floodplains as occur in the Biebrza River catchment. The Biebrza River catchment is a natural, temperate zone floodplain with fen wetlands, which is a reference site for wetland research (Wassen et al., 2006). The significant Biebrza wetland is a Ramsar and EU Natura 2000 listed site and has a status of national park in Poland. To verify the spatiotemporal dynamics, we compare the water sources data set obtained from field sampling against equivalent results of the HMC method. We hypothesize that the active perirheic zone exhibits considerable spatiotemporal dynamics, which are dependent on the consecutive and simultaneous occurrence of processes producing water from different sources, and subsequently, that the active perirheic zone is highly sensitive to any changes to the hydrological drivers of the system.

2. Materials and Methods

In order to explore the spatiotemporal dynamics of the active perirheic zone in the Biebrza River catchment we conducted a complex series of steps summarized in Figure 1.

2.1. Study Area

The Biebrza River catchment was selected as a study area because of its perirheic conditions in the lower basin (Keizer et al., 2014), which we hereafter refer to as the floodplain subarea (Figure 2). Also, the Biebrza floodplain is a reference site for comparable wetlands and fens because of its undisturbed river network, shallow groundwater levels, and low atmospheric deposition of nitrogen (Wassen et al., 2006). The floodplain constitutes about 250 km^2 of wetlands covered by meadows, reeds, forests, bushes, and their mosaics (Berezowski et al., 2018a). Soils in the floodplain are mostly organic with river sediments near the river channel, whereas the upland is covered mostly by glacial deposits such as sands and glacial tills. The geology of the floodplain was investigated along five cross sections, which disclose that the Quaternary deposits range usually between 60 to 140 m thickness with mostly sand, sand with gravel, till, and some clay; peat lays at the top with a thickness of up to 2 m (Banaszuk, 2004). A number of boreholes in the upland area of the Biebrza catchment reveal that the lithology is dominated by various tills and sands up to a depth of 10 to −60 m above mean sea level (amsl) (Polish Geological Institute, 2014). The climate is humid continental

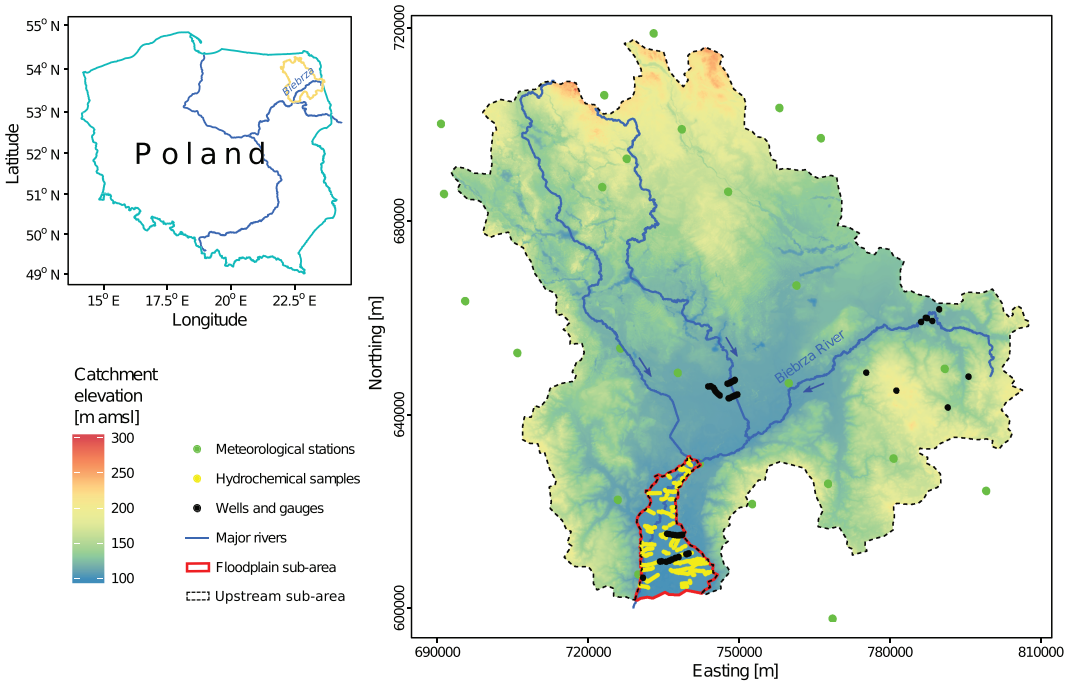

Figure 2. Location of the study area, the Biebrza River catchment. The HMC floodplain subarea is indicated by red polygon and the upstream subarea is indicated by black dashed polygon. Indicated are wells for head measurements and discharge gauges, meteorological stations, and hydrochemical sampling points.

according to the Köppen classification, while the Biebrza River exhibits typical spring floods. The average daily discharge for 1951–2017, measured at the section located near the Biebrza River outlet, was 34.7 m^3/s, with a minimum of 4.33 m^3/s and a maximum of 517 m^3/s.

2.2. Hydrological Modeling

The simulation of transient surface-subsurface flow of water was conducted using the HydroGeoSphere (HGS) model (Brunner & Simmons, 2012; Hwang et al., 2014). HGS is a fully integrated hydrological model that solves variably saturated 3-D water flow in a porous medium using a modified formulation of Richards equation and a two-dimensional depth-averaged surface water flow using the diffusive wave approximation to the Saint-Venant equations (Aquanty, 2013). This formulation allows investigation of groundwater-surface water interactions without a priori definition of active flow generation processes. Instead, simulated surface water-groundwater interactions are the result of simulated hydraulic head gradients and physical properties of the porous media and surface domains.

The model mesh was generated using the triangle code (Shewchuk, 1996) with the preprocessing and post-processing steps conducted according to the protocol provided in Kaser et al. (2014). The mesh included major streams and lakes, localization of the observation wells, and the sampling points for the hydrochemical analysis. The spatial domain of the model is the entire Biebrza River catchment, which comprises 7,092 km^2 (Figure 2). The mesh consisted of 253,540 nodes and 432,348 triangular prism elements (i.e., 36,220 nodes and 72,058 triangular elements per layer) and the area of the modeling domain was 7,085 km^2. The mesh was irregular, and 25% of the elements were smaller than 320 m^2 and 75% of the elements were smaller than 5,177 m^2, the median was 742 m^2. The larger elements were located in the flat, upland regions, whereas the smaller elements were located in the floodplain and the floodplain-upland margin.

A 20-m resolution "bare earth" digital elevation model (DEM) was obtained from the DEM of Poland (1:26,000), contours of the Topographic Map of Poland (1:25,000), and geodetic field surveys in the floodplain. The DEM was further updated with the lakes bathymetry. The riverbed elevation was separately interpolated based on a sounding conducted in 25 transects located in the lower and upper sections of the Biebrza River. The surface lithology was obtained from the geological map of Poland in scales 1:500,000 and 1:20,000 (the latter available for the floodplain only). The vertical representation of the geological strata was obtained from nine geological cross sections available for the entire river valley and adjacent parts of the

upland (Banaszuk, 2004) and elsewhere from several bore profiles managed by the Polish Geological Institute. The porous materials were generalized into three classes: low hydraulic conductivity glacial tills, high hydraulic conductivity sands, and peat. Land cover classes used to differentiate the evapotranspiration and overland flow properties were obtained from the Corine Land Cover database (Commission of the European Communities, 2013).

The model consisted of seven layers with gradually increasing thickness. The top four layers were relatively thin, from 25 to 100 cm thick in the floodplain. This vertical discretization resulted in usually four unsaturated layers in the floodplain-upland margin where most of the groundwater discharge took place. Within the floodplain the top layer was fully saturated for most of the flooding period. During very dry periods, at the end of the simulation, the saturation decreased to 40% in the first layer and 90% in the second layer. The vertical extent of the unsaturated zone was highly variable within the model domain: in the upland it could reach up to more than 20 m, whereas in the floodplain up to 1 m in relatively dry and elevated areas. The elevation of the top layer ranged from 98 to 275 m amsl, while the bottom layer had a constant elevation of −30 m amsl, which corresponded to the average lower boundary of the Quaternary sediments in the study area (Banaszuk, 2004).

The model was forced by the following boundary conditions: rain (specified flux in the top projection), snowmelt (specified flux based on snowfall and the degree-day method; Rango and Martinec (1995), Schilling et al., 2019), potential evapotranspiration (ET) (with actual evaporation and transpiration calculated based on root depth, soil moisture and leaf area index evolution over time; Kristensen and Jensen, 1975) and river water critical depth (at the model outlet). The daily time series of rain and snowmelt were obtained from 25 precipitation stations and four temperature stations (Figure 2). The daily potential ET data were obtained from the JRC AGRI4CAST database (Joint Research Center, 2014). The interpolated surfaces of the meteorological variables were obtained by kriging using the methodology presented in Berezowski et al. (2016). Precipitation was interpolated using universal kriging combined with indicator kriging in order to preserve zero precipitation areas in the output. The potential ET was interpolated using universal kriging. Both for precipitation and potential ET the exponential variogram model was used. Due to the snowmelt model implementation in HGS the temperature was provided as time series for individual stations and the contributing area of each station was established using the Thiessen polygons method.

The implemented formulation of the boundary conditions have several advantages. The precipitation and the potential ET series are relatively easy to measure, or estimate with reasonable uncertainty (although, the snowmelt calculation requires the degree-day model parameters estimation). Defining the modeling domain to the whole catchment allows setting no-flow boundary conditions at the nodes lying at the watershed boundary. Hence, this approach does not assume conditioning on any groundwater heads, by assuming negligible transcatchment groundwater flow. The critical depth boundary condition at the catchment outlet does not define any discharge or water level series constraining the model. However, the critical depth never occurs near the outlet of the Biebrza River and may cause unnatural hydrological behavior (e.g., too low water levels near the outlet). In order to limit the impacts of this behavior the critical depth boundary condition is moved 4 km downstream along the river from the last observation point used in the analysis of simulation results.

Variable time stepping is applied in solution of the flow equations, with time step duration adjusted based on predefined conditions, for example, maximum number of flow solver iterations, maximum head change, and maximum relative or absolute error. Full list of the conditions used are available, along with other model setup information, in the input GROK file (supporting information section S2), whereas, the full list of conditions is available in the model manual (Aquanty, 2013). The maximum time step allowed was set to 84600 s, but during the simulation the time steps range was between 0.11 and 12804 s with the median of 2,500 s. The shortest time steps were present at the beginning of the simulation and during the largest discharge events, whereas the longest since the end of the flood till the end of the simulation.

2.2.1. Model Calibration and Validation

The calibration period was one water year (1 November 1999 to 31 October 2000) with a 5-month warm-up period. The validation was conducted for the water year 2002. The year 2001 was omitted due to unusually low flow. The model parameters were identified based on 420 runs for 16 parameters with random, uniformly distributed values (Table 1). The script used to conduct the calibration was written in the R language

Table 1
Parameters Identified During the Model Calibration

Parameter	Search range	Value of calibrated parameter	Units
Van Genuchten model inverse of the air-entry pressure head	1.8 : 4.0	Peat: 3.51	m^{-1}
		Glacial till: 2.79	
		Sand: 3.73	
Van Genuchten model pore size distribution index	0.8 : 3.5	Peat: 1.83	—
		Glacial till: 1.65	
		Sand: 2.94	
Saturated hydraulic conductivity	5×10^{-8} :1×10^{-4}	Peat: 2.13×10^{-7}	ms^{-1}
		Glacial till: 1.00×10^{-6}	
		Sand: 9.27×10^{-5}	
Manning roughness coefficient	0.015 : 0.25	Biebrza channel: 0.039	$ms^{-\frac{1}{3}}$
		Crop: 0.076	
		Wetland and grassland: 0.066	
		Forest: 0.175	
Rill storage	1×10^{-4}: 1×10^{-4}	Wetland and grassland: 0.0014	m
		Forest: 0.0017	
Interception storage factor	1×10^{-4} : 1×10^{-2}	All land covers: 0.0018	m

and is available, along with sample data, in the supporting information section S3. For calibration and validation we used 54 observation wells, of which three were logging the heads automatically at a daily resolution, whereas the rest were manually read at 10- to 15-day intervals. Some of the wells were sporadically not accessed due to too high water levels or ice cover. We also used water level measurements from four household wells located in the upland in which the water level was read two to three times a year; water extraction from these wells was negligible. The daily discharge data were obtained from a water gauge located 4 km upstream from the model outlet. The criterion for model selection was to minimize the root-mean-square error [m]:

$$RMSE = \sqrt{\frac{\sum_{i=1}^{N}\left(h_i - \hat{h}_i\right)^2}{N}} \tag{1}$$

between observed (h_i) and simulated ($\hat{h}_i$) heads in wells for N time steps i and to maximize Kling-Gupta efficiency [-] (Gupta et al., 2009):

$$KGE = \sqrt{(r-1)^2 + (\alpha - 1)^2 + (\beta - 1)^2} \tag{2}$$

for discharge at the catchment outlet, where r is the correlation coefficient between simulated and observed discharge and α and β are ratios of simulated to observed mean and standard deviation discharges, respectively. Optimal RMSE is 0 and optimal KGE is 1. Spatial distribution of the wells and gauges is presented in Figure 2.

2.3. The Hydraulic Mixing-Cell Method Application

The mixture of water sources in each computational node of the model was calculated using the HMC method (Partington et al., 2011, 2013). The water sources have to be predefined and differentiated by area (e.g., subcatchments and landscape forms) and boundary conditions (e.g., rain and snowmelt). HMC calculation depends only on computed nodal water fluxes and does not require any extra parameters. Usually, all nodes are initialized with an artificial "initial" fraction equal to 1. In the subsequent time steps the water

sources fraction are mixed according to volumes of water flowing into and out of a cell:

$$f_{i(k)}^{t} = \left(\frac{V_i^{t-1}}{V_i^{t}} - \frac{Vbc_{out}^{t} + \sum_{j=1}^{m} V_{ij} \Big|_{t-1}^{t}}{V_i^{t}} \right) f_{j(k)}^{t-1} + \frac{Vbc_{k}^{t} + \sum_{j=1}^{n} V_{ij} \Big|_{t-1}^{t} f_{j(k)}^{t-1}}{V_i^{t}} \quad (3)$$

where there are n sources and m sinks for cell i; $f_{j(k)}^{t-1}$ [-] denotes fraction k at time $t-1$ in the neighboring cell j, V denotes the volume with the superscript denoting time state and subscript i denoting the cell, ij denoting volume into cell j from cell i over the time step from $t-1$ to t, ji denoting volume from neighbor j into i, and Vbc_k^t is a volume from the inflowing boundary condition associated with fraction k and Vbc_{out}^t is a volume summed from all outflowing boundary conditions at cell i.

Using the HMC method, we defined four sources of water with respect to a flood generation process, that is, (1) groundwater, (2) rain, (3) snowmelt, and (4) the previous year's water (i.e., the "initial" fractions) representing the water residing in the entire catchment from the previous water year. Further, we defined two subareas (Figure 2) to differentiate the HMC fractions spatially:

1. a floodplain subarea, which corresponds to the lower Biebrza floodplain (see Figure 2), where according to former studies the perirheic zone is extensive;
2. an upstream subarea that is a complement of the floodplain in the catchment area and which generates water that reaches the floodplain either via the river network or surface runoff.

As a result, we obtained at each model node the composition of seven HMC fractions (k in equation (3)): the groundwater $f_{groundwater\ floodplain}$, rain $f_{rain\ floodplain}$, and snowmelt $f_{snowmeltf\ loodplain}$ fractions generated in the floodplain subarea, $f_{groundwater\ upstream}$, $f_{rain\ upstream}$, and $f_{snowmelt\ upstream}$ fractions generated in the upstream subarea and the previous year fractions $f_{previous\ yr}$, which due to HMC implementation cannot be differentiated spatially.

2.4. Identification of the Active Perirheic Zone

Identification of the active perirheic zone is complicated due to its nature of being an effect of transient mixing of river and floodplain water. Hence, rather than delineating a discrete extent of the active perirheic zone, we use a continuous measure that quantifies a degree of river and floodplain water mixing (d) [-]:

$$d = 1 - \frac{|f_{\text{river}} - f_{\text{floodplain}}|}{1 - f_{\text{previous yr}}} \quad (4)$$

where $f_{\text{river}} = f_{groundwater\ upstream} + f_{rain\ upstream} + f_{snowmelt\ upstream}$ and $f_{\text{floodplain}} = f_{groundwater\ floodplain} + f_{rain\ floodplain} + f_{snowmelt\ floodplain}$; that is, they are river and floodplain water fractions calculated as a sum of groundwater, rain, and snowmelt HMC fractions for each model node generated respectively in the floodplain and upstream subareas. Notably, the f_{river} includes water generated not only in the Biebrza River but also in the tributaries and at the hillslopes of the floodplain margin as expressed by the upstream subarea. Therefore, this study characterizes the active perirheic zone without limiting its extent to only the Biebrza River channel (i.e., to the main channel of the system). To remove the effect of previous year water in the calculation, we normalize the absolute difference using the previous year HMC fractions ($f_{\text{previous yr}}$). In this formulation, a value of $d = 1$ is obtained if river and floodplain water fractions are equal in a model cell (i.e., perfect mix) and the value decreases toward $d = 0$ with one of the fractions being higher than the other one (i.e., nonperfect mix). For further analysis we calculate d for each time step and each model cell based on daily nodal f_{river} and $f_{floodplain}$ values; however, we drop the temporal and nodal indices in equation (4) for clarity.

In this study we interpret high degree of mixing values ($d > 0.75$) as an indicator for an active perirheic zone. The active perirheic zone corresponds to the dynamic boundary between the homogeneous patches of different water sources in the entire perirheic zone within an inundated floodplain as described by Mertes (1997).

2.5. Inundated Area Threshold

Water depth in the top layer of the model domain is continuously higher than 0 m. Yet, most of the time, in the area outside streams and lakes the depth is negligible (e.g., $\%1 \times 10^{-6}$ m). In order to recognize the inundated nodes in this study a subjective threshold for minimum water depth was set at 0.0025 m. This value

allowed to filter out areas briefly covered by water due to instantaneous fluxes, for example, precipitation or snowmelt. At the same time, the threshold preserved the shape of the inundation area and coverage in agreement with knowledge of the study area.

2.6. Composition of Inundation

To obtain an overview of temporal changes of inundation composition with respect to different water sources in the floodplain, we aggregate spatially the HMC fractions. The time series of floodplain area percentage ($\bar{A}_w$) [%] and within floodplain volume (V_w) [m^3] of water sources were calculated for w representing: *river*, *floodplain*, *previous yr*, *groundwater floodplain*, *snowmelt floodplain*, and *rain floodplain* (see sections 2.3 and 2.4):

$$\bar{A}_w = \frac{\sum_{m=1}^{M} f_{m,w} a_m}{\sum_{n=1}^{N} a_n} \times 100\% \tag{5}$$

$$V_w = \sum_{m=1}^{M} f_{m,w} a_m h_m \tag{6}$$

where n is a floodplain node from 1 to N and m is an inundated floodplain node from 1 to M, a_m and a_n are respectively contributing areas of node m or n calculated using the Thiessen polygon method, h_m is water depth of node m, and $f_{m,w}$ is fraction of water source w at node m. For calculation of the active perirheic zone area percentage ($\bar{A}_d$) [%] and volume (V_d) [m^3] within the floodplain we use a similar approach as in equations (5) and (6):

$$\bar{A}_d = \frac{\sum_{m=1}^{M} d_m a_m}{\sum_{n=1}^{N} a_n} \times 100\% \tag{7}$$

$$V_d = \sum_{m=1}^{M} d_m a_m h_m \tag{8}$$

however, the d_m(the degree of mixing d at node m) is used instead of $f_{m,w}$for weighting. This is justified by the fact that according to equation (4), d is calculated solely from the HMC fractions and has the same units. Therefore, in spite of the mixing degree d is not the same as fractions, d quantifies the intensity of a phenomenon and can be used as a weight.

2.7. Validation of the HMC Water Sources Fractions

The ground truth water sources locations in the lower Biebrza floodplain were identified based on hydrochemical analysis of 548 water samples acquired during the spring flood from 21 February 2002 to 16 March 2002 (Figure 2). The water samples were taken from inundation surface water and analyzed for 19 parameters: pH, electrical conductivity, organic carbon, and concentration of 16 ions. For the sake of water sources identification the data set was subjected to K-means clustering, yielding six output clusters: Biebrza River and tributaries, Wissa River (one of tributaries) only, groundwater, polluted groundwater, precipitation (snowmelt and rain), and polluted precipitation. Elaboration of the complete methodology for obtaining this data set is presented in Chormański et al. (2011). For further analysis in this paper we generalized the six clusters into three: river water, groundwater, and precipitation.

2.7.1. Statistical Tests

The HMC method provides fractions ($f^t_{j(k)}$) of water sources in each node of the model (i.e., real numbers), which cannot be easily cross tabulated with the discrete water sources clusters ground truth. Therefore, we conducted Kruskal and Wallis (1952) statistical test (H statistics), which verify whether the distribution of the HMC fractions are different in the groups defined by the water source clusters. The H statistic is calculated as

$$H = \frac{12}{N(N+1)} \sum_{i=1}^{C} \frac{R_i^2}{n_i} - 3(N+1) \tag{9}$$

where C is the number of samples, n_i is the number of observations in the ith sample, $N = \sum n_i$, is the number of observations in all samples combined, and R_i is the sum of the ranks in the ith sample (Kruskal & Wallis, 1952). We also conducted a post hoc Dunn (1964) test (Z statistics) to check which distributions of HMC fractions differ within a hydrochemical cluster. The Z statistic for two groups A and B, which are in our case a pair of hydrochemical clusters used to group the HMC fractions, is calculated as

$$Z = \frac{\frac{R_A}{n_A} - \frac{R_B}{n_B}}{\sqrt{\left(\frac{N(N+1)}{12} - \frac{\sum_{s=1}^{w} \omega_s^3 - \omega_s}{12(N-1)}\right)\left(\frac{1}{n_A} + \frac{1}{n_B}\right)}} \tag{10}$$

where R_A and R_B are the Groups A and B summed ranks, n_A and n_B are Groups A and B sample size, w is the total number of tied ranks, and ω_s is the number of observations in the sth tied rank. The Dunn's test p values were corrected for multiple comparisons using the Holm (1979) procedure.

First, we expect that the fraction distributions will be different between the clusters, which would confirm that the different composition of water in clusters is reflected by fractions. We also expect that the distributions of the fractions will exhibit the following pattern; that is, the medians will have the highest values in the appropriate clusters, for example, river in the river cluster, snowmelt, or rain in the precipitation cluster and groundwater in groundwater cluster. This pattern would confirm that the dominant water source indicated by fractions agrees with the labels of each cluster. In addition, we also test whether the distribution of a particular fraction is different between the three clusters. This test would verify if a particular fraction plays a role in differentiating between water sources. For each test we used the HMC fractions from a model node matching the sampling point and from a day corresponding to the sampling day of the respective hydrochemical sample. This allows us to verify the HMC results both in space and time.

The Kruskal-Wallis and Dunn tests were used, because they are nonparametric and not strict about the input data. Analysis of variance (ANOVA) with Tukey's post hoc test could not be used in our case, because the experiment was not balanced. Yet, the statistical tests were taken under the assumption that the sampling points for water sources clusters were chosen at representative locations for the study area. Therefore, we sampled a relatively large number of locations (548) distributed all over the floodplain (Figure 2) and covering all water sources.

2.7.2. Random Forests Pattern Fitting

We also verified whether the simulated HMC fractions can be used to reproduce the ground truth hydrochemical clusters pattern. This was achieved by training a machine learning algorithm Random Forest (Breiman, 2001) to recognize (fit) the clusters based on HMC fractions. This approach yields a best fitted water source class to the HMC fractions in each node overlying a hydrochemical sampling point. We verify the fit using the bootstrap-based out-of-bag error [%] produced by Random Forest, which is an unbiased estimator of the training set error (Breiman, 2001). We also calculated a confusion matrix with overall accuracy understood as a percentage of correctly fitted locations from all sampling locations and per class reliability and accuracy. The accuracy estimates the probability that a given class in the study area is classified correctly, while the reliability estimates the probability that an object classified into a given class indeed belongs to a given class. The confusion matrix is calculated using the test sample, because we are interested in estimating how accurate this particular fit can be, rather than building a prediction model which would have to be verified based on an independent sample.

3. Results

3.1. Hydrological Modeling

The simulated heads were characterized by an RMSE of 0.279 m (17.5% of the maximum difference between wells maximum and minimum head) and match well the overall hydraulic gradient in the study area (r^2 of 0.998). The simulated discharge yielded a KGE of 0.807, which reflected the minor mismatch between the simulated and observed discharge hydrograph, such as an imperfect timing and magnitude of the two flood peaks, and a small discharge peak at the beginning of the simulation (Figure 3).

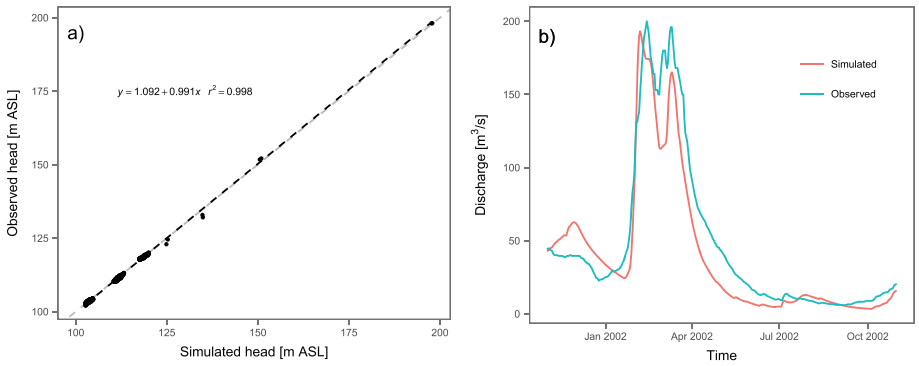

Figure 3. Verification of the integrated hydrological model for the Biebrza River catchment. (a) Simulated and observed heads for 54 wells ($N = 1,935$), gray line is a 1:1 line. (b) Simulated and observed daily ($N = 365$) discharge at the Burzyn gauging station (~4 km from the model outlet). The calibration period is not plotted.

3.2. Validation of the HMC Water Sources Fractions

The distributions of simulated HMC fractions (herein referred to as just "fraction(s)") were significantly different in the water source clusters (Figure 4). The outcome of the statistical tests was confirmed by visual comparison, where high fraction values are present in the location of corresponding clusters during the three sampling sessions (Figure 5). The snowmelt and rain fractions had expected patterns; that is, their medians were the highest in the precipitation cluster and the same was observed for the river fraction in the river cluster (Figure 4a). The groundwater fraction did not follow this pattern (Figure 4a). However, the groundwater fraction had a higher median in the groundwater cluster than in the precipitation and river clusters and the difference between groundwater and river fractions was significant (Figure 4b). Rain and snowmelt fractions displayed similar distributions in groundwater and precipitation clusters but at the same time they were significantly different from the river fractions distribution (Figure 4b). The previous year's water fraction was significantly different in each cluster (Figure 4b) with the highest median in the river cluster. However, previous year's water distribution was not significantly different from the river fraction in the river cluster (Figure 4a).

The Random Forest algorithm fitted the hydrochemical clusters pattern using the fractions with 28.47% out-of-bag error. The overall accuracy of the fit as expressed by the confusion matrix was 72% (Table 2). The river and precipitation obtained acceptable per-class accuracy and reliability. However, the fit of the groundwater fractions had 59% reliability and only 51% accuracy.

3.3. Spatiotemporal Dynamics of the River Water, Floodplain Water, and Active Perirheic Zone

River and floodplain water coverage had a similar order of magnitude in terms of maximum share in the floodplain area, but the maximum floodplain water volume was only ~38% of the maximum river water volume (Figures 6b and 6c, January/February 2002). The river water peaks persisted longer than floodplain water peaks; they also developed and decayed at lower rate than the floodplain water in terms of both volume and area (Figures 6b and 6c). The active perirheic water area percentage $\bar{A}_d$ had similar dynamics

Table 2
Confusion Matrix Between the Random Forest Fit Using Simulated Fractions and the Ground Truth Hydrochemical Clusters Expressed in Number of Sampling Points

	Random Forest fit			
Ground truth clusters	Groundwater	Precipitation	River	Accuracy
Groundwater	50	37	12	51%
Precipitation	27	138	32	70%
River	8	40	204	81%
Reliability	59%	64%	82%	Overall acc. = 72%

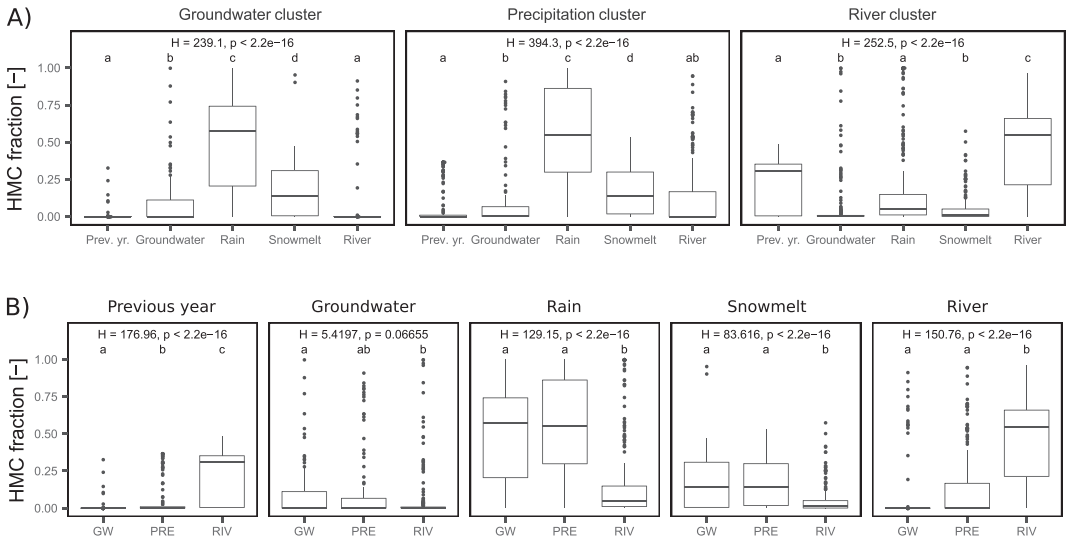

Figure 4. Simulated fraction distributions grouped by HMC endmembers in the three hydrochemical clusters (a) and simulated fraction distributions grouped by the three hydrochemical clusters in the five HMC endmembers (b). Both panels presents the same data, however, differently grouped. The plots are labeled with the value of Kruskal-Wallis H statistics accompanied by its p value. The letters a, b, c, and d indicate the post hoc Dunn's test distribution differences at $p < 0.05$, that is, different letters stand for different distributions and the same letters stand for the same distribution (no significant differences). GW is groundwater, PRE is precipitation, and RIV is river hydrochemical cluster.

as the floodplain water $\bar{A}_{f\,floodplain}$ in except that its peak was ~50% of $\bar{A}_{f\,floodplain}$ (Figure 6c, January–March 2002). The active perirheic water volume, V_d, that was strongly correlated ($r = 0.93$) to the floodplain water $V_{floodplain}$ correlation with river water V_{river} was weaker ($r = 0.57$). The components of $V_{floodplain}$ were correlated with V_d as follows: $V_{snowmel\,floodplain}$ ($r = 0.84$), $V_{rain\,floodplain}$ ($r = 0.77$), and $V_{groundwater\,floodplain}$ ($r = 0.21$). The total fluxes per unit area show that majority of water was provided to the surface model domain by rain: 415 mm, while the snowmelt accounted for 133 mm and groundwater discharge for 13 mm (Figure S2). Up to ~10% of inundation area was covered by water from previous year $\bar{A}_{previous\ year}$ (Figure 6c), which due to the limitation of the 1-year period of analysis cannot be labeled as river or floodplain water.

The spatiotemporal dynamics of river, groundwater, snowmelt, and rain fractions, presented in section S1, effectively determined the active perirheic zone presence as indicated using the degree of mixing measure—d (Figure 6a). At the beginning of the flood (21 January 2002) the active perirheic zone was located at the margins of the inundation and along major drainage ditches that connects the river with the zone of groundwater discharge at the floodplain boundary. Ten days later (31 January 2002), at the beginning of the flood peak, the active perirheic zone was present in a nearly entire 2- to 5-km belt along the Biebrza River with d values decreasing northwise. Just before the flood event started to decline (22 March 2002) the active perirheic zone extent was similar as to the beginning of the flood. A difference was that the inundation extent was larger and the active perirheic zone formed a frontier rather than a patch along the river. After the end of the flood event (21 May 2002) the active perirheic zone extent was limited only to the negative relief distributed in various areas of the floodplain and to the margins of river water shallow inundation, located along the Biebrza River.

The precise definition of an area in which the active perirheic zone moved in the entire floodplain is difficult due to the heterogeneity of the system and a lack of reference points. Our cross-section analysis revealed that during the flooding period the frontier could move in Cross Section 1 within an ~1,000-m buffer zone around its position at the beginning of the flood (i.e., in the buffer situated 700 to 1,700 m from the river; Figure 7), whereas in Cross Section 2 clear frontiers are within a narrower (100–300 m) buffer distanced ~700 m from the river, appearing on both sides of the river (Figure 7). In both cross sections the active perirheic zone was reappearing in previous occupied locations, for example, at 700–1,000 m east to the river in the Cross Section 1 and 500–700 m east to the river in the Cross Section 2.

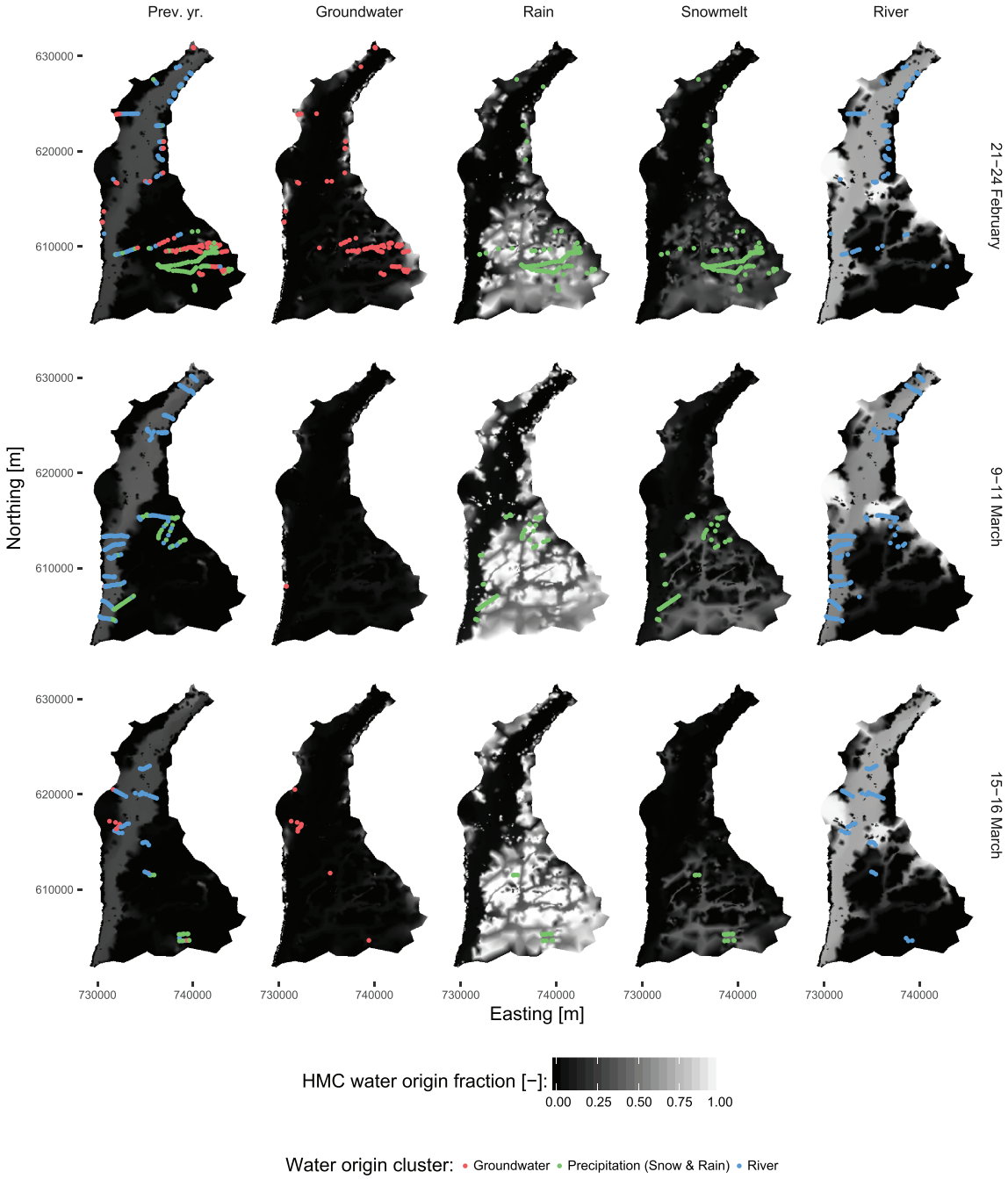

Figure 5. Spatiotemporal verification of HMC fractions by ground truth hydrochemical clusters in the Biebrza floodplain subarea during the verification period: 1 November 2001 to 31 October 2002. The HMC fractions of groundwater, snowmelt, rain, river, and previous year water (columns) are overlaid by points presenting the hydrochemical clusters sampled during three campaigns (rows). The previous year water fraction is overlaid by all hydrochemical clusters. The HMC fraction maps present the daily values from the central day of the hydrochemical sampling campaign, that is, 22 February 2002 (top panels), 10 March 2002 (middle panels), and 16 March 2002 (bottom panels).

The distribution of maximum d values calculated during the flooding period (10 January 2002 to 01 May 2002) showed that only 26% of the floodplain had a degree of mixing of $d = 0$. At the same time, the high degrees of mixing, $d > 0.75$, were present in 38% of the floodplain.

The largest volume of active perirheic water was observed during the flood rising (20 January 2002 to 26 February 2002; Figure 6b). During this period the floodplain area with $d = 0$ was the same as for the flooding period and the high degree of mixing, $d > 0.75$, was present in 34% of the floodplain (Figures 8c and 8d).

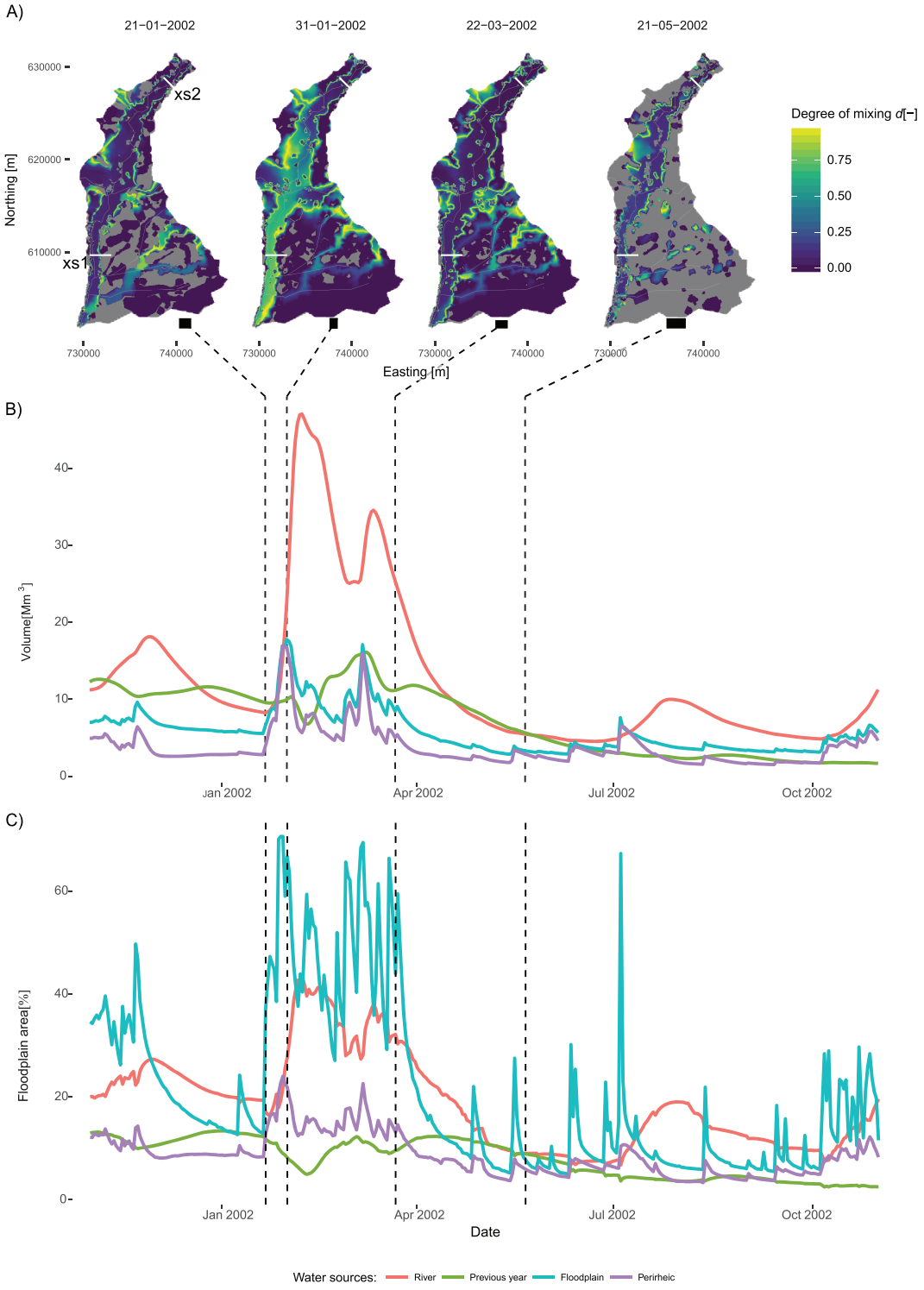

Figure 6. Spatiotemporal dynamics of the active perirheic zone in the Biebrza floodplain subarea. The top panel (a) presents the spatial pattern of mixing (d) during flooding period. Gray background indicates no inundation; gray lines indicate rivers and major drainage ditches; white lines and labels indicate location of two cross sections (xs1 = southern and xs2 = northern, Figure 7) used for further analysis; outlet is located in the southeastern corner of the valley. The bottom panels present the temporal changes of the volume (b) and area (c) for the river, floodplain (groundwater, rain, and snowmelt), active perirheic, and previous year water in the floodplain subarea. Calculations of area percentages and volume were made using equations (5–8).

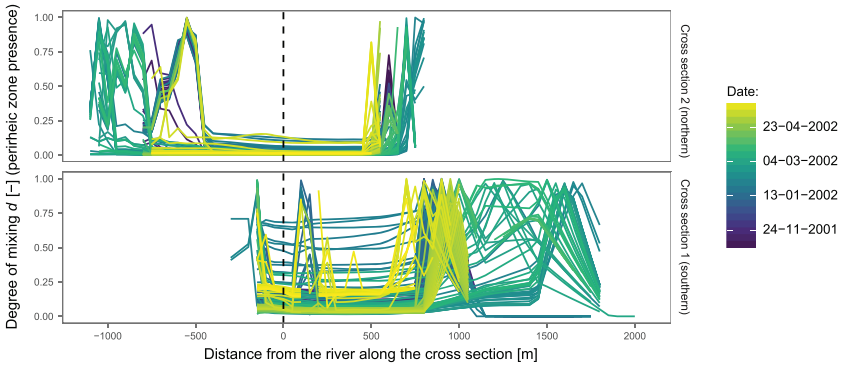

Figure 7. Spatiotemporal dynamics of the active perirheic zone captured at two cross sections in the Biebrza floodplain subarea (Figure 6a). The lines present the degree of mixing (d) variation along the cross sections as time lapse. The Biebrza River is located at 0-m position and is indicated using the dashed line; negative numbers indicate distance left (west) of the river, and positive values indicate distance right (east) of the river. Empty line segments indicate no inundation.

During the ten day period from 26 January 2002 to 04 February 2002 the points of maximum d shifts with distance of up to 500 m onto the floodplain from its initial location at the boundary of the river water dominated extent (Figures 8a and 8b, including the zoomed area therein). This spatiotemporal dependency is less visible in the remote part of the floodplain, where the day of maximum d appears in large, homogeneous patches at various points in time (Figure 8a).

4. Discussion

4.1. Hydrological Modeling and HMC Fractions

Our hydrological model verification showed very good overall performance, which gives us confidence in the HMC results and the simulated spatiotemporal dynamics of the active perirheic zone. In our case study the error figures indicate an appropriate fit, similar to those reported in other transient state studies using the HGS model (Alaghmand et al., 2016; Glaser et al., 2016; Schepper et al., 2017). Nonetheless, we observed some mismatch between observations and simulated heads and discharge. We attribute these features to drawbacks of the degree-day snowmelt model included in HGS, which effectively caused an earlier appearance of the first flood peak and a lower magnitude of the second peak. Decreased simulated discharge in the first 2 months of the simulation was an influence of the initial conditions. This negative influence could potentially be decreased if a longer (e.g., 2 years) warm-up period were used; however, this would increase already very long run times and calibration of the model. Partially, the errors can be attributed to the use of homogeneous parameters for hydrogeologic and surface units and due to generalization of river geometry in the model mesh. Applying finer elements and including heterogeneous parameter fields within hydrogeologic and surface units would likely improve the simulation accuracy. However, this is again a trade-off with the model run and calibration times.

Additionally, to the verification for heads and discharge, we verified the HMC results using the hydrochemical data set. Statistical analysis of the distribution of all fractions for precipitation and river clusters were as expected; that is, the fractions had the highest medians in the corresponding hydrochemical clusters. Random Forests pattern fitting also indicated good agreement. Hence, the results can be used as a marker of dominant water sources in a given study area. The groundwater fraction had the highest median in the groundwater cluster. However, the distribution of the remaining fractions in the groundwater cluster did not follow expectation and the Random Forests pattern fitting indicated poor agreement for groundwater. Therefore, with respect to groundwater dominated inundation our results did not agree with Chormański et al. (2011) and Keizer et al. (2014) where hydrochemical clusters in Biebrza were labeled according to expert interpretation followed by statistical analysis. According to our simulation the groundwater flux to the surface was too low to make groundwater a dominant water source in an extensive part of the floodplain. The simulated average groundwater flux in a node labeled as groundwater cluster is −0.1 mm/day (i.e., infiltration) and 0.9 mm/day maximum, which is relatively low when compared to the average

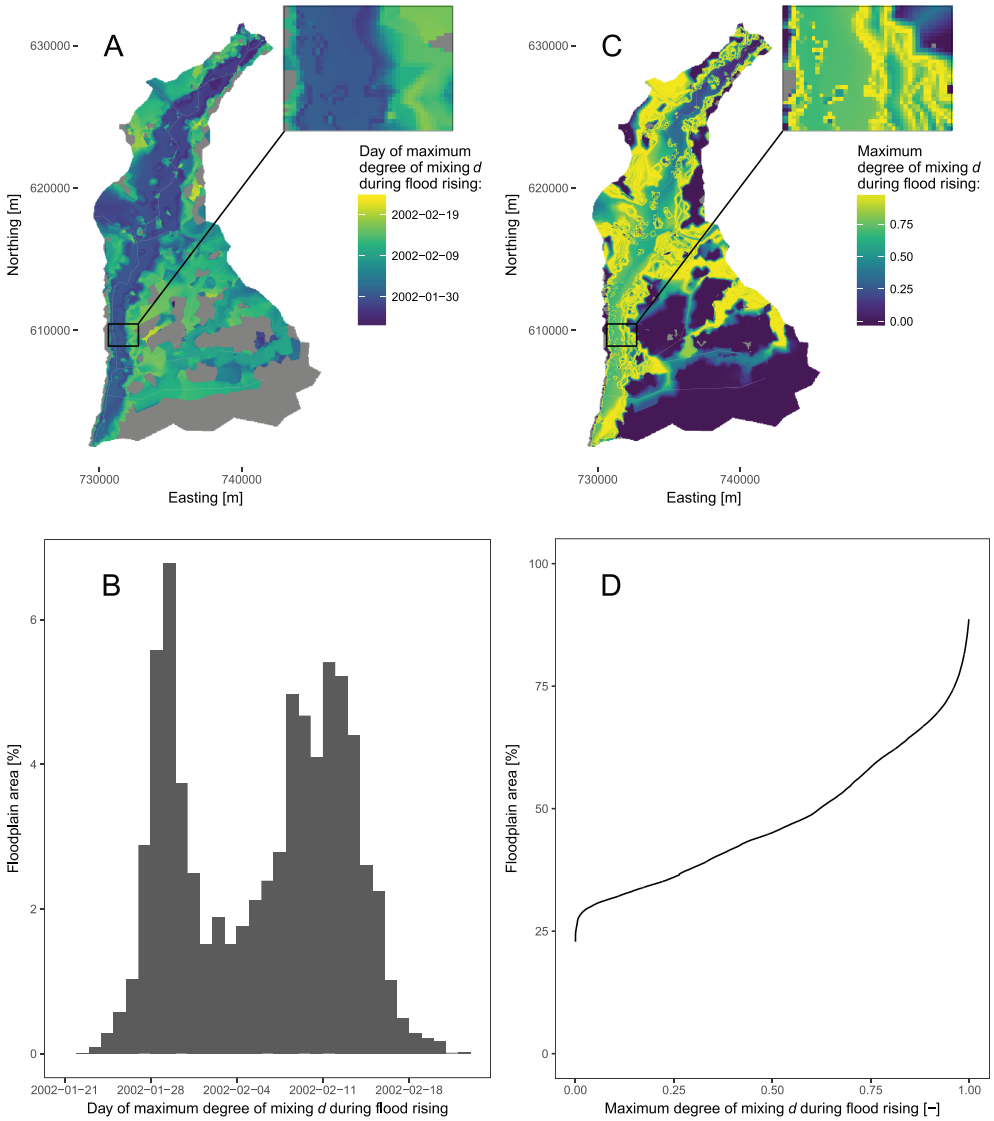

Figure 8. Behavior of the active perirheic zone during the flood rising period (20 January 2002 to 26 February 2002) expressed as maximum degree of mixing (d) measure properties. The panels present the day of maximum d occurrence as a map (a) and as a histogram (b) and the corresponding maximum value of d as a map (c) and as a cumulative distribution (d). Extent of the 2.1 × 1.6-km zoomed area in panels (a) and (c) is centered at Cross Section 1. High d values indicate the presence of the active perirheic zone.

precipitation of 1.2 mm/day. Effectively, according to our simulations, inundation in groundwater discharge areas was diluted by precipitation or snowmelt, which had higher volumes. The signal of groundwater discharge was evident in the groundwater clusters; however, the low values of groundwater fractions could not unequivocally confirm that the model nodes were dominated by groundwater.

On the other hand, the elevated groundwater fraction values could be responsible for the signal received by hydrochemical analysis in the groundwater clusters. To confirm our reasoning we also looked at behavior of other floodplains. The simulated processes in the floodplain were in agreement with experiments carried out by Beumer et al. (2007) in Dutch floodplains. As shown in their study, groundwater did not produce extensive inundation through significant discharge fluxes. Rather, it saturated the soil pores prior to a flood and prevented infiltration of water from the river or precipitation.

4.2. Use of the HMC Method for Water Sources Mapping

The most important limitation of applying the HMC method is the need for a physically based, distributed, hydrological model. If water fluxes simulated by a model are erroneous the HMC water fractions will be

of course misleading. Therefore, accurate model identification, reflected in, for example, high accuracy of simulated heads and fluxes, is required for HMC applications.

On the other hand, the HMC method, which computes the composition of water from any predefined sources at an appropriate spatiotemporal resolution can be complementary to currently used field sampling and remote sensing by helping to overcome their limitations. Field sampling is labor-intensive and time-consuming. Moreover, differentiation between the water sources (e.g., between snowmelt, ice melt, glacier melt, or rain) requires elaborate approaches such as isotope analysis for separation (e.g. Maurya et al., 2011; Penna et al., 2014), or conceptual hydrological modeling (Weiler et al., 2017). Remote sensing techniques (Mertes, 1997; Park & Latrubesse, 2015) are less labor-demanding, but so far applied only to differentiate between sediment-rich and sediment-poor waters and are limited by sensor overpass timing, spatial resolution, or obscuring of an object of interest by, for example, vegetation.

4.3. The Active Perirheic Zone Dynamics

The volume of river water exchange to the floodplain was almost threefold higher than the total volume of floodplain water in Biebrza, which agrees with a dominating contribution of river water to flood volume reported for other perirheic floodplains (Bonnet et al., 2017; Rudorff et al., 2014b). Yet, we showed that the temporal dynamics of the active perirheic water volume in Biebrza floodplain during the single-year study period was more related to water sources driven by local meteorological forcing rather than to upstream river discharge. The volume of snowmelt (133 mm per unit area) water was lower than rainfall water (415 mm per unit area). Counterintuitively, the correlation coefficients between the volume of different water sources within the floodplain depicted that the snowmelt played a more important role in the active perirheic zone dynamics (r =0.84) than rain (r = 0.77). Groundwater had clearly the lowest volume of the analyzed water sources and its impact on the active perirheic zone dynamics was low. Nonetheless, it had a role in surface wetting and saturating the floodplain soil pores that promotes inundation by rain and snowmelt in the initial phase of the flood (Beumer et al., 2007). It is possible that the sensitivity of the active perirheic zone to the longer memory of the groundwater system was not captured in the single-year analysis.

Nearly all floodplain water volume contributed to the active perirheic zone. However, due to extensive shallow inundation in the remote parts of the Biebrza floodplain, the area of active perirheic zone was 50 percentage points lower than the area of floodplain water when comparing the highest peaks (Figures 6a, 6c, and S1).

Our results show that Biebrza River water and floodplain water do not mix extensively on the floodplain and that the active perirheic zone was primarily present at the river-floodplain water frontier (Figure 6a). The observed occurrence of the active perirheic zone on the floodplain was also influenced by small tributaries and surface runoff from upland hillslopes (section S1), which also mixed with the floodplain water. The effective volume of the mixing was, however, negligible in comparison to the Biebrza River-floodplain water frontier.

In the Biebrza floodplain the maximum daily active perirheic zone extent was 24% (Figure 6). However, when taking into account the spatiotemporal dynamics 38% of the floodplain was covered with a high degree of mixing during the flooding period. Furthermore, the active perirheic zone can appear in the same place more than one time. The active perirheic zone covered 34% of the floodplain already during the early period of flood development, when the most dynamic behavior occurs, in particular, intensive snowmelt followed by rain showers. Within this period the high degree of mixing was observed both at the Biebrza River-floodplain water frontier and at the floodplain where minor tributaries are located and surface runoff from upland to the floodplain discharges. For 26% of the floodplain area no floodplain and river water mixing occurred due to topography, distance to the river network, and distance to the floodplain-upland border. To summarize, despite a relatively local extent of the active perirheic zone at a given time moment and no perirheic water occurrence in some places, during the entire flooding period its extent was up to 160% larger than the maximum daily extent.

Due to the described dynamics, various processes related to the perirheic zone, such as nutrient cycling (Jones et al., 2014; Racchetti et al., 2011; Scott et al., 2014) including its relation to floodplain ecology (Kaller et al., 2015; Keizer et al., 2014, 2018; Walalite et al., 2016) and also sedimentation or erosion (Aalto et al., 2003; Lewin et al., 2017; Park & Latrubesse, 2015; Shellberg et al., 2013), will vary spatiotemporally in their dynamics within a floodplain area and cannot be considered static. Therefore, our findings support Bonnet

et al. (2017), who analyzed the water balance in a part of Amazonian floodplain. As they recommend, the physicochemical and biogeochemical processes in an inundated floodplain field sampling should be conducted at an appropriate spatial and temporal resolution. Clearly, the method presented in this study can help guiding or even partially replace field sampling.

The local rain, snowmelt, and groundwater discharge fluxes changed their magnitude consecutively or in turns to initiate and sustain inundation and effectively produce the active perirheic zone. In analogy to the alteration of temperature, precipitation, snowmelt, and groundwater pattern influence the timing and magnitude of flood and drought (Garner et al., 2015; Van Loon et al., 2015) this complex flux pattern may be sensitive to reduction in some of the fluxes at a required magnitude or timing. Effectively this may result in failure in producing the required amount of inundation for development of the active perirheic zone or change its pattern.

Future climate change is expected to change the water resources, flood, and drought risk (Alcamo et al., 2007; Hirabayashi et al., 2013; Lehner et al., 2006). Therefore, the dependence of the active perirheic zone on the local hydrological and climatic conditions has obvious implications under climate change and should be investigated in future climate change effect analyzes.

5. Conclusions

In the Biebrza floodplain, groundwater, snow, rain, and river water contribute in a complex pattern to inundation and form the active perirheic zone that moves from the river's edge onto the floodplain and back toward the river during the flooding period. Primarily, this movement was observed within a 1-km buffer from the initial active perirheic zone location. The active perirheic zone was also present in remote parts of the floodplain due to surface runoff at the floodplain-upland boundary and due to discharge of small tributaries. During the entire flooding period, the active perirheic zone moved over 38% of the floodplain, which is 160% larger than its maximum daily extent (24% of the floodplain area). No mixing of floodplain and river water occurred in 26% of the floodplain. Effectively, the biogeochemical or hydrogeomorphological processes coupled to the active perirheic zone are not static but dynamic in space and time. We therefore, stress the importance of capturing the dynamics of the active perirheic zone through selection of appropriate spatial and temporal resolutions and appropriate tools for investigating these processes, with the benefit of a complementary modeling and field study demonstrated here.

The perirheic zone is present in many of the world's floodplains, and this study provides a first detailed description of the active perirheic zone's spatiotemporal dynamics. We expect that the dynamics of the active perirheic zone, as highlighted in Biebrza, will be prevalent in similar floodplains. The dominant drivers of the active perirheic zone are, however, study site dependent. In the Biebrza floodplain the active perirheic zone dynamics were driven by the floodplain water rather than river water. The most important drivers within the floodplain water were snowmelt and rain. Because of that the active perirheic zone in Biebrza is sensitive to the hydrological regime, is climate dependent, and is thus likely vulnerable to climate change and to other factors influencing the water balance.

For future research, in parallel to field studies, we recommend exploration of the active perirheic zone dynamics through complementary scenario modeling (e.g., climate change or land use and water management oriented) and also as a feedback for other Earth system models focused on biogeochemical, ecological, or hydrogeomorphological processes.

Acknowledgments
This research was partially supported by Grant 2017/26/D/ST10/00665 funded by the National Science Centre, Poland. The integrated hydrological modeling results including the HMC results are available in Berezowski et al. (2018b); the hydrochemical data set is available in Chormański et al. (2011). Spatial and hydrometeorological data for modeling were obtained from Biebrza National Park, Poland, JRC AGRI4CAST, and Institute of Meteorology and Water Management-National Research Institute (IMGW-PIB), Poland. Numerical modeling was conducted on eResearch South Australia cluster. Authors are greatfull to two anonymous reviewers for deep comments that led to great improvement of this paper.

References

Aalto, R., Maurice-Bourgoin, L., Dunne, T., Montgomery, D. R., Nittrouer, C. A., & Guyot, J.-L. (2003). Episodic sediment accumulation on Amazonian flood plains influenced by El Nino/Southern Oscillation. *Nature*, *425*(6957), 493–497.

Alaghmand, S., Beecham, S., Woods, J., Holland, K., Jolly, I., Hassanli, A., & Nouri, H. (2016). Quantifying the impacts of artificial flooding as a salt interception measure on a river-floodplain interaction in a semi-arid saline floodplain. *Environmental Modelling & Software*, *79*, 167–183.

Alcamo, J., Flörke, M., & Märker, M. (2007). Future long-term changes in global water resources driven by socio-economic and climatic changes. *Hydrological Sciences Journal*, *52*(2), 247–275.

Aquanty (2013). HydroGeoSphere User Manual. Waterloo, Canada: Aquanty Inc.

Banaszuk, H. (2004). Kotlina Biebrzanska i Biebrzanski Park Narodowy. Bialystok: Ekonomia i Srodowisko. in Polsih

Bates, P., & De Roo, A. (2000). A simple raster-based model for flood inundation simulation. *Journal of Hydrology*, *236*(1-2), 54–77.

Berezowski, T., D. Partington, J. Chormański, & Batelaan, O. (2018b), Surface water source fractions and hydraulic heads for Biebrza River catchment in water year 2002, https://doi.org/10.4121/uuid:b6245d75-0908-43ae-97ce-8f58f3ae8f48.

Berezowski, T., Szcześniak, M., Kardel, I., Michałowski, R., Okruszko, T., Mezghani, A., & Piniewski, M. (2016). CPLFD-GDPT5: High-resolution gridded daily precipitation and temperature data set for two largest Polish river basins. *Earth System Science Data*, *8*(1), 127–139.

Berezowski, T., Wassen, M., Szatyłowicz, J., Chormański, J., Ignar, S., Batelaan, O., & Okruszko, T. (2018a). Wetlands in flux: looking for the drivers in a central European case. *Wetlands Ecology and Management*, *26*(5), 849–863.

Beumer, V., van Wirdum, G., Beltman, B., Griffioen, J., & Verhoeven, J. (2007). Biogeochemical consequences of winter flooding in brook valleys. *Biogeochemistry*, *86*(1), 105–121.

Bonnet, M.-P., Pinel, S., Garnier, J., Bois, J., Boaventura, G. R., Seyler, P., & Marques, D. M. (2017). Amazonian floodplain water balance based on modelling and analyses of hydrologic and electrical conductivity data. *Hydrological Processes*, *31*(9), 1702–1718.

Breiman, L. (2001). Random forests. *Machine Learning*, *45*(1), 5–32.

Brunner, P., & Simmons, C. T. (2012). Hydrogeosphere: A fully integrated, physically based hydrological model. *Ground Water*, *50*(2), 170–176.

Chormański, J., Okruszko, T., Ignar, S., Batelaan, O., Rebel, K., & Wassen, M. (2011). Flood mapping with remote sensing and hydrochemistry: a new method to distinguish the origin of flood water during floods. *Ecological Engineering*, *37*(9), 1334–1349.

Commission of the European Communities (2013), Corine land-cover, date accessed: 2013-10-12.

Dunn, O. J. (1964). Multiple comparisons using rank sums. *Technometrics*, *6*(3), 241–252.

Forshay, K. J., & Stanley, E. H. (2005). Rapid nitrate loss and denitrification in a temperate river floodplain. *Biogeochemistry*, *75*(1), 43–64.

Freeze, R., & Harlan, R. (1969). Blueprint for a physically-based, digitally-simulated hydrologic response model. *Journal of Hydrology*, *9*(3), 237–258.

Fritz, K. M., Schofield, K. A., Alexander, L. C., McManus, M. G., Golden, H. E., Lane, C. R., et al. (2018). Physical and chemical connectivity of streams and riparian wetlands to downstream waters: A synthesis. *JAWRA Journal of the American Water Resources Association*, *54*(2), 323–345.

Garner, G., Loon, A. F. V., Prudhomme, C., & Hannah, D. M. (2015). Hydroclimatology of extreme river flows. *Freshwater Biology*, *60*(12), 2461–2476.

Glaser, B., Klaus, J., Frei, S., Frentress, J., Pfister, L., & Hopp, L. (2016). On the value of surface saturated area dynamics mapped with thermal infrared imagery for modeling the hillslope-riparian-stream continuum. *Water Resources Research*, *52*, 8317–8342. https://doi.org/10.1002/2015WR018414

Gupta, H. V., Kling, H., Yilmaz, K. K., & Martinez, G. F. (2009). Decomposition of the mean squared error and nse performance criteria: Implications for improving hydrological modelling. *Journal of Hydrology*, *377*(1-2), 80–91.

Hirabayashi, Y., Mahendran, R., Koirala, S., Konoshima, L., Yamazaki, D., Watanabe, S., et al. (2013). Global flood risk under climate change. *Nature Climate Change*, *3*(9), 816–821.

Holm, S. (1979). A simple sequentially rejective multiple test procedure. *Scandinavian Journal of Statistics*, *6*(2), 65–70.

Hwang, H.-T., Park, Y.-J., Sudicky, E., & Forsyth, P. (2014). A parallel computational framework to solve flow and transport in integrated surface subsurface hydrologic systems. *Environmental Modelling & Software*, *61*, 39–58.

Joint Research Center (2014), Agri4Cast Resources Portal, date accessed: 2014-11-02.

Jones, C. N., Scott, D. T., Edwards, B. L., & Keim, R. F. (2014). Perirheic mixing and biogeochemical processing in flow-through and backwater floodplain wetlands. *Water Resources Research*, *50*, 7394–7405. https://doi.org/10.1002/2014WR015647

Junk, W., P. B. Bayley, and R. E. Sparks (1986), The flood pulse concept in river-floodplain systems, in *International large river symposium*.

Kaller, M., Keim, R., Edwards, B., Raynie Harlan, A., Pasco, T., Kelso, W., & Allen Rutherford, D. (2015). Aquatic vegetation mediates the relationship between hydrologic connectivity and water quality in a managed floodplain. *Hydrobiologia*, *760*(1), 29–41.

Kaser, D., Graf, T., Cochand, F., McLaren, R., Therrien, R., & Brunner, P. (2014). Channel representation in physically based models coupling groundwater and surface water: Pitfalls and how to avoid them. *Groundwater*, *52*(6), 827–836.

Keizer, F., der Lee, G. V., Schot, P., Kardel, I., Barendregt, A., & Wassen, M. (2018). Floodplain plant productivity is better predicted by particulate nutrients than by dissolved nutrients in floodwater. *Ecological Engineering*, *119*, 54–63.

Keizer, F., Schot, P., Okruszko, T., Chormanski, J., Kardel, I., & Wassen, M. (2014). A new look at the flood pulse concept: The (ir)relevance of the moving littoral in temperate zone rivers. *Ecological Engineering*, *64*(0), 85–99.

Kollet, S. J., & Maxwell, R. M. (2006). Integrated surface-groundwater flow modeling: A free-surface overland flow boundary condition in a parallel groundwater flow model. *Advances in Water Resources*, *29*(7), 945–958.

Kristensen, K. J., & Jensen, S. E. (1975). A model for estimating actual evapotranspiration from potential evapotranspiration. *Hydrology Research*, *6*(3), 170–188.

Kruskal, W. H., & Wallis, W. A. (1952). Use of ranks in one-criterion variance analysis. *Journal of the American Statistical Association*, *47*(260), 583–621.

Lehner, B., Döll, P., Alcamo, J., Henrichs, T., & Kaspar, F. (2006). Estimating the impact of global change on flood and drought risks in Europe: A continental, integrated analysis. *Climatic Change*, *75*(3), 273–299.

Lewin, J., Ashworth, P. J., & Strick, R. J. P. (2017). Spillage sedimentation on large river floodplains. *Earth Surface Processes and Landforms*, *42*(2), 290–305.

Li, L., Lambert, M. F., Maier, H. R., Partington, D., & Simmons, C. T. (2015). Assessment of the internal dynamics of the australian water balance model under different calibration regimes. *Environmental Modelling & Software*, *66*, 57–68.

Li, L., Maier, H., Lambert, M., Simmons, C., & Partington, D. (2013). Framework for assessing and improving the performance of recursive digital filters for baseflow estimation with application to the lyne and hollick filter. *Environmental Modelling & Software*, *41*, 163–175.

Li, L., Maier, H. R., Partington, D., Lambert, M. F., & Simmons, C. T. (2014). Performance assessment and improvement of recursive digital baseflow filters for catchments with different physical characteristics and hydrological inputs. *Environmental Modelling & Software*, *54*, 39–52.

Liggett, J. E., Partington, D., Frei, S., Werner, A. D., Simmons, C. T., & Fleckenstein, J. H. (2015). An exploration of coupled surface-subsurface solute transport in a fully integrated catchment model. *Journal of Hydrology*, *529*, 969–979.

Liggett, J. E., Werner, A. D., Smerdon, B. D., Partington, D., & Simmons, C. T. (2013). Fully integrated modeling of surface-subsurface solute transport and the effect of dispersion in tracer hydrograph separation. *Water Resources Research*, *50*, 7750–7765.

Maurya, A. S., Shah, M., Deshpande, R. D., Bhardwaj, R. M., Prasad, A., & Gupta, S. K. (2011). Hydrograph separation and precipitation source identification using stable water isotopes and conductivity: River Ganga at Himalayan foothills. *Hydrological Processes*, *25*(10), 1521–1530.

Mertes, L. A. K. (1997). Documentation and significance of the perirheic zone on inundated floodplains. *Water Resour. Res.*, *33*(7), 1749–1762.

Mertes, L. A. K. (2000). Inland Flood Hazards: Human, Riparian, and Aquatic Communities, chap. Inundation Hydrology, (pp. 145–166). Cambridge, UK: Cambridge University Press.
Park, E., & Latrubesse, E. M. (2015). Surface water types and sediment distribution patterns at the confluence of mega rivers: The Solimões-Amazon and Negro Rivers junction. *Water Resources Research*, *51*, 6197–6213. https://doi.org/10.1002/2014WR016757
Partington, D., Brunner, P., Frei, S., Simmons, C. T., Werner, A. D., Therrien, R., et al. (2013). Interpreting streamflow generation mechanisms from integrated surface-subsurface flow models of a riparian wetland and catchment. *Water Resources Research*, *49*, 5501–5519. https://doi.org/10.1002/wrcr.20405
Partington, D., Brunner, P., Simmons, C., Therrien, R., Werner, A., Dandy, G., & Maier, H. (2011). A hydraulic mixing-cell method to quantify the groundwater component of streamflow within spatially distributed fully integrated surface water-groundwater flow models. *Environmental Modelling & Software*, *26*(7), 886–898.
Partington, D., Brunner, P., Simmons, C., Werner, A., Therrien, R., Maier, H., & Dandy, G. (2012). Evaluation of outputs from automated baseflow separation methods against simulated baseflow from a physically based, surface water-groundwater flow model. *Journal of Hydrology*, *458-459*, 28–39.
Penna, D., Engel, M., Mao, L., Dell'Agnese, A., Bertoldi, G., & Comiti, F. (2014). Tracer-based analysis of spatial and temporal variations of water sources in a glacierized catchment. *Hydrology and Earth System Sciences*, *18*(12), 5271–5288.
Polish Geological Institute (2014), Ikar geoportal.
Racchetti, E., Bartoli, M., Soana, E., Longhi, D., Christian, R. R., Pinardi, M., & Viaroli, P. (2011). Influence of hydrological connectivity of riverine wetlands on nitrogen removal via denitrification. *Biogeochemistry*, *103*(1), 335–354.
Rango, A., & Martinec, J. (1995). Revisiting the degree-day method for snowmelt computations. *JAWRA Journal of the American Water Resources Association*, *31*(4), 657–669.
Rudorff, C. M., Melack, J. M., & Bates, P. D. (2014a). Flooding dynamics on the lower amazon floodplain: 1. Hydraulic controls on water elevation, inundation extent, and river-floodplain discharge. *Water Resources Research*, *50*, 619–634. https://doi.org/10.1002/2013WR014091
Rudorff, C. M., Melack, J. M., & Bates, P. D. (2014b). Flooding dynamics on the lower amazon floodplain: 2. Seasonal and interannual hydrological variability. *Water Resources Research*, *50*, 635–649. https://doi.org/10.1002/2013WR014714
Scaroni, A. E., Nyman, J. A., & Lindau, C. W. (2011). Comparison of denitrification characteristics among three habitat types of a large river floodplain: Atchafalaya River Basin, Louisiana. *Hydrobiologia*, *658*(1), 17–25.
Schepper, G. D., Therrien, R., Refsgaard, J. C., He, X., Kjaergaard, C., & Iversen, B. V. (2017). Simulating seasonal variations of tile drainage discharge in an agricultural catchment. *Water Resources Research*, *53*, 3896–3920. https://doi.org/10.1002/2016WR020209
Schilling, O., Gerber, C., Partington, D. J., Purtschert, R., Brennwald, M. S., Kipfer, R., et al. (2017). Advancing physically-based flow simulations of alluvial systems through atmospheric noble gases and the novel 37ar tracer method. *Water Resources Research*, *53*, 10,465–10,490. https://doi.org/10.1002/2017WR020754
Schilling, O. S., Park, Y.-J., Therrien, R., & Nagare, R. M. (2019). Integrated surface and subsurface hydrological modeling with snowmelt and pore water freeze-thaw. *Groundwater*, *57*(1), 63–74.
Scott, D. T., Keim, R. F., Edwards, B. L., Jones, C. N., & Kroes, D. E. (2014). Floodplain biogeochemical processing of floodwaters in the Atchafalaya River Basin during the Mississippi River flood of 2011. *Journal of Geophysical Research: Biogeosciences*, *119*, 537–546. https://doi.org/10.1002/2013JG002477
Sebben, M. L., Werner, A. D., Liggett, J. E., Partington, D., & Simmons, C. T. (2013). On the testing of fully integrated surface-subsurface hydrological models. *Hydrological Processes*, *27*(8), 1276–1285.
Shellberg, J. G., Brooks, A. P., Spencer, J., & Ward, D. (2013). The hydrogeomorphic influences on alluvial gully erosion along the Mitchell River fluvial megafan. *Hydrological Processes*, *27*(7), 1086–1104.
Shewchuk, J. (1996). Triangle: Engineering a 2D quality mesh generator and delaunay triangulator. In M. Lin, & D. Manocha (Eds.), Lecture Notes in Computer Science, (Vol. 1148, pp. 203–222). Berlin Heidelberg: Springer.
Van Loon, A. F., Ploum, S. W., Parajka, J., Fleig, A. K., Garnier, E., Laaha, G., & Van Lanen, H. A. J. (2015). Hydrological drought types in cold climates: quantitative analysis of causing factors and qualitative survey of impacts. *Hydrology and Earth System Sciences*, *19*(4), 1993–2016.
VanderKwaak, J. E., & Loague, K. (2001). Hydrologic-response simulations for the R-5 catchment with a comprehensive physics-based model. *Water Resources Research*, *37*(4), 999–1013.
Walalite, T., Dekker, S. C., Keizer, F. M., Kardel, I., Schot, P. P., deJong, S. M., & Wassen, M. J. (2016). Flood water hydrochemistry patterns suggest floodplain sink function for dissolved solids from the Songkhram monsoon river (Thailand). *Wetlands*, *36*(6), 995–1008.
Wassen, M. J., Okruszko, T., Kardel, I., Chormanski, J., Swiatek, D., Mioduszewski, W., et al. (2006). Eco-hydrological functioning of the Biebrza wetlands: Lessons for the conservation and restoration of deteriorated wetlands. *Wetlands: Functioning, Biodiversity Conservation, and Restoration*, *191*, 285–310.
Weiler, M., Seibert, J., & Stahl, K. (2017). Magic components-why quantifying rain, snowmelt, and icemelt in river discharge is not easy. *Hydrological Processes*, *32*(1), 160–166. https://doi.org/10.1002/hyp.11361
Wilson, M., Bates, P., Alsdorf, D., Forsberg, B., Horritt, M., Melack, J., et al. (2007). Modeling large-scale inundation of Amazonian seasonally flooded wetlands. *Geophysical Research Letters*, *34*, L15404. https://doi.org/10.1029/2007GL030156

Erratum

In the originally published version of this article, Table 1 contained formatting errors. The table has been corrected and this version may be considered the authoritative version of record.